

ARTICLE

Effect of Fluorination on the Crystal Structure, Stability and Gas Adsorption Property in Zinc(II) Metal-organic Frameworks^①

ZHANG Xin CHEN Zhen-Xia

YANG Yong-Tai DENG Ming-Li^② WENG Lin-Hong

(Shanghai Key Laboratory of Molecular Catalysis and Innovative Materials,
Department of Chemistry, Fudan University, Shanghai 200433, China)

ABSTRACT Three zinc(II) metal-organic frameworks (**xF-MAC-3**) have been synthesized by using Zn(II) salts, 3,5-dimethyl-1*H*-1,2,4-triazole (Hdmtz) and different fluorination degree carboxylate ligands, which are analogic structures and can be described as (6,6)-connected *pcu*-b net. We find that the fluorine atoms have structural regulation effect on **xF-MAC-3**, which can not only enlarge the torsion angle φ of carboxylate ligands but also elevate the space group of structures. Besides, the CO₂-273 K uptake increased from 23.21 cm³·g⁻¹ (**MAC-3**) to 36.13 cm³·g⁻¹ (**4F-MAC-3**) and H₂-77 K uptake increased from 24.33 cm³·g⁻¹ (**MAC-3**) to 59.79 cm³·g⁻¹ (**4F-MAC-3**), which means fluorination can enhance the gas adsorption uptake of **xF-MAC-3** analogues. Furthermore, the results of fluorination in **xF-MAC-3** analogues offer a potential way to study the ligand pre-functionalization effect on the structures and properties of MOFs analogues.

Keywords: metal-organic frameworks, fluorine functionalization, X-ray crystallography, gas adsorption;
DOI: 10.14102/j.cnki.0254-5861.2011-3264

1 INTRODUCTION

Metal-organic frameworks (MOFs) are porous crystalline materials which are constructed by secondary building units (SBUs) and organic ligands^[1-3]. In the last two decades, due to their permanent porosity, structural stability and easily functionalization, MOFs have been widely studied in the fields of applications such as gas adsorption and purification^[4-6], catalysis^[7-9], molecule sensing and recognition^[10-12].

Since fluorine atoms have the strongest electronegativity and small electron polarization, introducing fluorine-containing functional groups into MOFs can change the pore channel properties and lead to various applications^[13-15], such as hydrocarbon separation^[16-19], ionic conductivity^[20] and, mostly important, H₂ and CO₂ adsorption^[21-23]. Nevertheless, fluorination will largely change the acidity and coordination ability of the carboxylate ligand, so that fluorinated analogues of MOFs constructed by carboxylate ligands can hardly be

synthesized^[24-26]. In recent years, some fluorinated analogues of MOFs have been synthesized and the effects of fluorination on MOFs have been studied^[27-29]. However, there are still some challenges to figure out the effect of fluorination in MOFs for crystal structures, stabilities, H₂ and CO₂ adsorption properties, which arouses our interests.

Cheetham and co-workers investigated that a series of 3D fluorinated-MOFs can be synthesized by using perfluorinated carboxylates in combination with nonfluorinated nitrogen heterocyclic ligands such as imidazole^[30], triazole^[31], and both bipyridine^[32]. Inspired by this, we synthesized three analogic structures (**xF-MAC-3**) based on our previous work^[33] by using Zn(II) salts, 3,5-dimethyl-1*H*-1,2,4-triazole (Hdmtz) and different fluorination degree carboxylate ligands. We also discuss the effects of fluorination on MOFs structure, thermal and chemical stability, H₂ and CO₂ adsorption properties in detail.

Received 22 May 2021; accepted 23 July 2021 (CCDC 2085003 and 2085109)

① This research was supported by the NSFC (No. 21971045), Natural Science Foundation of Shanghai (No. 18ZR1402900), the National Key Technologies R&D Program of China (2017YFA0205103), and Shanghai Leading Academic Discipline Project (B108)

② Corresponding author. Deng Ming-Li, associated professor, majoring in inorganic chemistry. E-mail: mldeng@fudan.edu.cn

2 EXPERIMENTAL

2.1 General materials and methods

All reagents were purchased from commercial sources and used without further purification, except for 3,5-dimethyl-1*H*-1,2,4-triazole (HDmtrz) and 2,5-difluoroterephthalic acid (H₂DFBDC), which were synthesized according to the references^[34, 35]. Fourier Transform Infrared Spectra (FT-IR) were performed on a ThermoFisher Nicolet iS10 FT-IR spectrometer in the range of 4000–400 cm⁻¹ with KBr pellets. Elemental analyses of C, N and H were tested on the Elementar Vario EL III. Powder X-ray diffraction (PXRD) was measured by using a Bruker D8 Advance diffractometer with Cu-*Kα* radiation ($\lambda = 1.5406 \text{ \AA}$). Thermogravimetric analyses (TGA) were carried out on SDT Q600 with the temperature range of 30–900 °C under N₂ flow at a heating rate 10 °C·min⁻¹. Gas adsorption analyses were tested on the Micromeritics ASAP 2020 surface area analyzer. Before gas sorption, the as-made MOF samples (about 100 mg) were exchanged with dichloromethane (10 mL for three times) and then degassed at 140 °C for 10 hours.

2.2 X-ray crystallographic study

Single-crystal X-ray diffraction (SC-XRD) of all compounds was performed on a Bruker D8 Venture MetalJet with Ga-*Kα* radiation ($\lambda = 1.3414 \text{ \AA}$) at 173 K. Data collection and reduction were performed with APEX III, and empirical absorption corrections were applied by the SADABS program. Structures were solved by direct methods using the SHELXS program and refined with the SHELXL program^[36]. Non-hydrogen atoms and N-bonded *H* atoms were directly obtained from a difference Fourier map. C-bonded H atoms were placed geometrically and refined as riding modes. Final refinements were carried out by full-matrix least-squares methods with anisotropic thermal parameters for all non-hydrogen atoms on *F*². SQUEEZE method was used to consider the disorder in the channel of the structures^[37].

2.3 Syntheses

2.3.1 3,5-Dimethyl-1*H*-1,2,4-triazole (HDmtrz)

Acetamide (60 g, 1 mol) and 80 wt% hydrazine hydrate (30 g, 0.5 mol) were added into a 250 mL flask and heated at 120 °C for 3 h, when the reaction solution first turned pink and then became colorless. After that, the reaction temperature was increased to 180 °C for 3 h and about 30 mL of liquid was distilled. Finally, the temperature was further increased to 240 °C and colorless liquid was distilled, which was condensed on the tube as white solid product (8.98 g, 0.09

mol). Yield: 9%. ¹H NMR (DMSO-*d*₆) showed $\delta = 13.13$ (s, 1H), 2.20 (s, 6H).

2.3.2 2,5-Difluoroterephthalic acid (H₂DFBDC)

2,5-Difluoro-4-methylbenzoic acid (5.6 g, 33.5 mmol), N-bromosuccinimide (NBS, 29.5 g, 165 mmol) and benzoyl peroxide (BPO, 0.4 g) were added into 100 mL CCl₄ and refluxed at 120 °C for 48 h and the reaction system changed into orange color. The hot mixture was filtered and washed successively with hot CCl₄, and the organic solution was extracted with 1 M HCl by three times, dried over anhydrous MgSO₄, filtered and evaporated. The remaining orange solid was the intermediate product with the mass of 9.14 g. ¹H NMR (DMSO-*d*₆): $\delta = 7.71$ (q, 1H), 7.61 (q, 1H), 7.41 (s, 1H).

The intermediate product (9.14 g) and sodium periodate (7.17 g, 33.5 mmol) were added into 50 mL 2% H₂SO₄ and refluxed at 90 °C for 24 h. The product was subsequently cooled to room temperature and the cold mixture was filtered, then the precipitate was washed with water. The solids were recrystallized from acetic acid to gain white powder 3.47 g (17.5 mmol). Yield: 52.2%. ¹H NMR (DMSO-*d*₆): $\delta = 7.68$ (t, 2H).

2.3.3 Zn₂(BDC)₂(Dmtrz)]·(CH₃NH₃)·2H₂O (MAC-3)

Zn(OAc)₂·2H₂O (75 mg, 0.2 mmol), terephthalic acid (H₂BDC, 33 mg, 0.2 mmol) and HDmtrz (10 mg, 0.1 mmol) were added to 10 mL *N,N*-dimethylformamide (DMF) and stirred for 10 min. Then the solution was sealed in a Teflon-lined stainless-steel autoclave (15 mL) and heated at 140 °C for 3 days, followed by cooling down to room temperature. Colorless block crystals were collected by filtration. Yield: 75% based on the Zn(OAc)₂·2H₂O. Elemental analysis calculated for **MAC-3** (Zn₂C₂₁H₂₄N₄O₁₀, 623.19): C, 40.41; N, 8.98; H, 3.85%. Found: C, 40.50; N, 9.41; H, 3.78%. FT-IR (cm⁻¹): 3426m, 3059m, 2963m, 2794m, 2484w, 1952w, 1632vs, 1599vs, 1492s, 1393vs, 1253w, 1136w, 1099m, 10118m, 875w, 816m, 753s, 694w, 592w, 514m (Fig. 1b).

2.3.4 Zn₃(H₂O)₂(MeO)₂(DFBDC)₂(Dmtrz)]·(CH₃)₂NH₂ (2F-MAC-3)

[Zn(NO₃)₂·6H₂O (87 mg, 0.3 mmol), H₂DFBDC (40 mg, 0.2 mmol) and HDmtrz (10 mg, 0.1 mmol) were added to the mixture solution of DMF (2 mL) and methanol (MeOH, 8 mL), and the mixture was stirred for 10 min. Subsequently, the mixture was sealed in a Teflon-lined stainless-steel autoclave (15 mL) and heated at 90 °C for 12 h, followed by cooling down to room temperature. Colorless block crystals were collected by filtration. Yield: 60% based on the Zn(NO₃)₂·6H₂O. Elemental analysis calculated for **2F-MAC-3** (Zn₃C₂₄H₂₈N₄O₁₂F₄, 836.61): C, 34.42; N, 6.69; H,

3.35%. Found: C, 34.45; N, 6.65; H, 3.30%. FT-IR (cm^{-1}): 3411m, 3073w, 2978m, 2927w, 2878w, 2448w, 2033w, 1646vs, 1588vs, 1486m, 1419vs, 1356s, 1264m, 1213m, 1183s, 1121m, 1026w, 988w, 945w, 900m, 853m, 808s, 774s, 706w, 657w, 529m (Fig. 1b).

2.3.5 $[\text{Zn}_2(\text{TFBDC})_2(\text{Dmtrz})]\cdot\text{H}_2\text{O}$ (**4F-MAC-3**)

$\text{Zn}(\text{NO}_3)_2\cdot 6\text{H}_2\text{O}$ (87 mg, 0.3 mmol), 2,3,5,6-tetrafluoroterephthalic acid (H_2TFBDC , 48 mg, 0.2 mmol) and HDmtrz (10 mg, 0.1 mmol) were added to the mixture solution of *N,N*-diethylformamide (DEF, 2 mL) and MeOH (8 mL), and the mixture was stirred for 10 min. Then the mixture was sealed in a Teflon-lined stainless-steel autoclave (15 mL) and heated at 90 °C for 12 h, followed by cooling down to room temperature. Light purple block crystals were collected by filtration. Yield: 65% based on $\text{Zn}(\text{NO}_3)_2\cdot 6\text{H}_2\text{O}$. Elemental analysis calculated for **4F-MAC-3** ($\text{Zn}_2\text{C}_{20}\text{H}_9\text{N}_3\text{O}_9\text{F}_8$, 718.04): C, 33.42; N, 5.84; H, 1.24%. Found: C, 33.50; N, 5.94; H, 1.20%. FT-IR (cm^{-1}): 3422m, 2921w, 2941w, 2874w, 2361w, 1639vs, 1474m, 1419vs, 1356s, 1264m, 1213m, 1183s, 1121m, 1026w, 988w, 945w, 900m, 853m, 808s, 774s, 706w, 657w, 529m (Fig. 1b).

3 RESULTS AND DISCUSSION

3.1 Synthesis and general characterization

$\text{Zn}_2(\text{BDC})_2(\text{Dmtrz})\cdot(\text{CH}_3\text{NH}_3)\cdot 2\text{H}_2\text{O}$ (**MAC-3**) was synthesized by solvothermal method in DMF with the raw material ratio of $\text{Zn}(\text{OAc})_2\cdot 2\text{H}_2\text{O}:\text{H}_2\text{BDC}:\text{HDmtrz}$ as 3:2:2 after referring to the previously reported method^[33]. However, we failed to acquire **xF-MAC-3** ($x = 2$ or 4) under the same synthesis conditions, which we believed that was mainly due to the introduction of fluorine atoms^[38]. Due to the strongest electronegativity and electron polarization of the fluorine atom, the electronic density on the benzene ring and the ligand acidity would change after the introduction of the fluorine atom into the carboxylate ligand. As the number of fluorine atoms increases, the electronic density of the benzene

ring would decrease while the ligand acidity would increase, which changed the coordination ability of the carboxylate ligand and affected the synthesis of MOF materials. Therefore, we used zinc nitrate with stronger coordination ability as the metal salt during the synthesis of **2F-MAC-3**. We also introduced methanol with low boiling point and strong polarity into the solvent system and used milder reaction conditions to gain high quality **2F-MAC-3** single crystal. During the synthesis of **4F-MAC-3**, we replaced DMF with DEF, which had better ligand solubility and helped to obtain the single-crystal test-qualified **4F-MAC-3** sample.

The PXRD pattern of **xF-MAC-3** samples fitted well with the simulated data, confirming the pure phase of all samples (Fig. 1a). The existence of fluorine atoms in the structures was checked by using ^1H NMR and FT-IR spectroscopy. The FT-IR spectra of **2F-MAC-3** and **4F-MAC-3** had absorption peaks at 1182 and 989 cm^{-1} , respectively, which could be ascribed as the stretching vibration peaks of C–F bonds, showing the presence of fluorine functionalized ligands (Fig. 1b)^[39]. Furthermore, the disappearance of C–H non-planar deviational vibration peaks in the range of 950~780 cm^{-1} in **4F-MAC-3** FT-IR spectrum also implied the absence of C–H bonds in **4F-MAC-3**, certifying that the carboxylate ligand in **4F-MAC-3** is TFBDC^[40]. The ^1H NMR spectroscopy showed the ligand composition of **xF-MAC-3** structures. The ^1H NMR spectra of **MAC-3** and **2F-MAC-3** had two NMR peaks with different chemical shifts, where the peak at δ 7.99 could be ascribed as the benzene ring hydrogen of carboxylate ligand (–PhH) and that at δ 2.48 was the methyl hydrogen of the Dmtrz ligand (–CH₃), respectively (Fig. 1c). The ratio of the two ligands closed to 1:1 calculated by the peak integrating area, which was consistent with the structural molecular formula results. There was only one peak in the ^1H NMR spectrum of **4F-MAC-3** at δ 2.44, which was the methyl hydrogen (–CH₃) of the Dmtrz ligand. The absence of other chemical shift peaks also proved that the carboxylate ligand in **4F-MAC-3** is TFBDC.

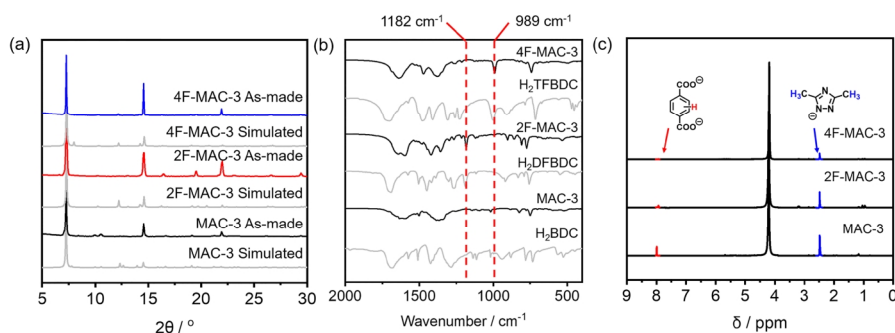


Fig. 1. (a) PXRD pattern; (b) FT-IR spectra; (c) ^1H NMR spectra of **xF-MAC-3** ($x = 0, 2, 4$)

3.2 X-ray crystal structure

As a prototype structure, single-crystal X-ray diffraction study revealed that **MAC-3** crystallized in monoclinic system, $C2/m$ space group (Table S1). The asymmetric unit of **MAC-3** contained two crystallographically independent Zn(II). Four carboxylate groups in BDC ligands and N atoms in Dmtrz ligands coordinated to Zn(1) and Zn(1)^A (A: $1-x, y, 2-z$), forming zinc paddle-wheel SBU $[Zn_2(COO)_4N_2]$. Two Dmtrz ligands coordinated to Zn(2) and Zn(2)^B (B: $1-x, 1-y, 1-z$) via

a $\mu_{1,2}$ -bridging mode to construct triazolate-dinuclear SBUs $[Zn_2(Dmtrz)_2O_4]$ (Fig. 2a). Two SBUs connected with each other to generate a 1D chain structure with a folding angle θ of 168.78° , and such chains are linked by BDC ligands along the x and y axes to form a 3D structure with a $7.0\text{\AA} \times 7.0\text{\AA}$ channel along the c axis (considering van der Waals radius, Fig. 2b). Considering paddle-wheel and triazolate-dinuclear as 6-connected SBUs, **MAC-3** could be defined as a (6,6)-connected *pcu-b* topology net (Fig. S1)^[41].

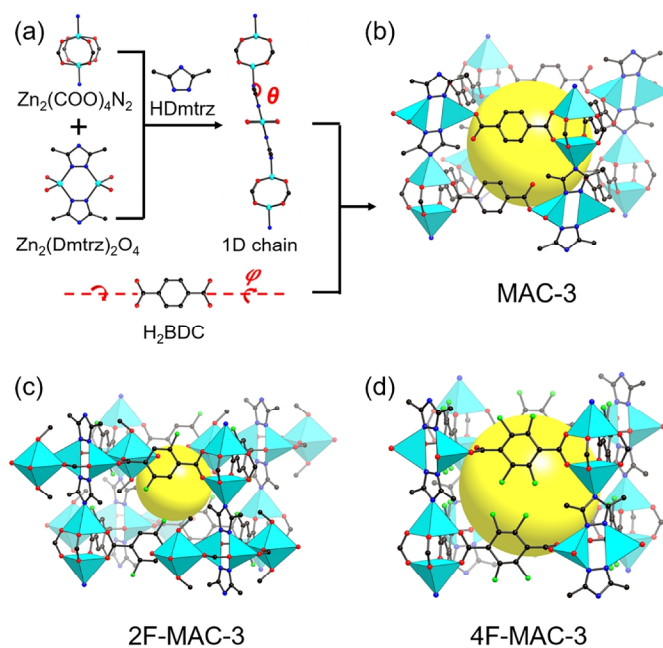


Fig. 2. (a) Secondary building units and organic ligands of *x*F-MAC-3; (b)–(d) Single-crystal structures of *x*F-MAC-3

Based on the **MAC-3** prototype structure, we replaced BDC ligand by fluorine-functionalized ligands to synthesize iso-structures and **2F-MAC-3** & **4F-MAC-3** were subsequently isolated (Fig. 2c, d, Fig. S2, 3 and Table S1). Distinct structural changes concerning the carboxylate ligands, 1D chain and SBUs are summarized in Table 1 and Fig. 1b, which mainly included (i) space group elevated from $C2/m$ (**MAC-3**) to $Immm$ (**2F-MAC-3** & **4F-MAC-3**); (ii) the folding angle θ of 1D chain changed from obtuse angle (168.78°) into straight angle (180°); (iii) the torsion angle φ in BDC ligands turned into right angle; (iv) triazolate-dinuclear SBU changed into a novel zinc tetranuclear SBU when the BDC ligand was replaced by fluorine-functionalized DFBDC ligands. The 1D channel size of **2F-MAC-3** is $4.0\text{\AA} \times 6.8\text{\AA}$ (considering van der Waals radius) which is smaller than **MAC-3**. The channel of **2F-MAC-3** is smaller than **MAC-3** mainly caused by the larger zinc tetranuclear SBU in **2F-MAC-3**, which reduced the size of 1D channel in MOFs. Furthermore, the 1D channel size of **4F-MAC-3** is $6.8\text{\AA} \times 6.8\text{\AA}$ (considering van der Waals

radius) which is slightly smaller than **MAC-3**. Considering the SBUs in **4F-MAC-3** are the same with **MAC-3**, the smaller 1D channel in **4F-MAC-3** is due to the relatively larger size of fluorine atoms.

There are two important differences in the chemistry of fluorine-functionalized BDC ligands compared to their nonfluorinated analogues, which caused the structural changes in *x*F-MAC-3 mentioned above. The first difference among three carboxylate ligands is the pK_a value. As discussed, the pK_a value of BDC-derived ligands decreases with the increasing number of fluorine atoms on the ligand, which means the acidities of **2F-MAC-3** & **4F-MAC-3** are stronger than **MAC-3**. So the fluorinated ligands can be deprotonated more easily and coordinated with zinc ions in a multidentate mode. This explains SBUs in **MAC-3** are paddle-wheel and triazolate-dinuclear when SBUs in **2F-MAC-3** & **4F-MAC-3** are paddle-wheel and zinc tetranuclear. Secondly, in **2F-MAC-3** & **4F-MAC-3**, the fluorine atoms of BDC ligands enlarge the torsion angle φ to a right angle, by which the

carboxylate groups are twisted out of the benzene ring. This can be attributed to (i) an electrostatic repulsion effect between the fluorine atoms on the benzene ring and the lone-pair oxygen atoms on the carboxylate groups; (ii) the decrease in aromatic character of BDC ligands due to the electron-withdrawing nature of the fluorine atoms^[42]. The two differences mentioned above cause the folding angle θ of 1D chain in **xF-MAC-3** ($x = 2, 4$) become a straight angle, thus inducing structures to crystallize in a higher symmetry space group (Fig. S4). This suggests that the introduction of fluorine atoms into ligand has a structure directing effect on the synthesized **xF-MAC-3**.

3.3 Structural stability

To study the porosity of **xF-MAC-3**, we first investigated the thermal and solvent stability of **xF-MAC-3** to determine the activation conditions for gas adsorption test. The TGA analysis reveals that all **xF-MAC-3** samples contain two weight loss peaks. The first one from room temperature to 200 °C shows about 25% weight loss, which can be attributed to the departure of guest molecules. The second weight loss peak from 250 to 600 °C results from the decomposition of the framework. For the increasing fluorination degree will weaken the C(-Phenyl)-C(Carboxylate) bond, the decarboxylation reaction will be easy to occur as the degree of fluorination increases, which makes the decomposition temperature significantly shift to lower temperature (420 °C for **MAC-3**

and 250 °C for **4F-MAC-3**, Fig. 3a)^[43]. From the variable temperature PXRD patterns of **xF-MAC-3**, we can find that the structures will keep the crystallinity until 180 °C, which is consistent with the TGA data (Fig. 3b-d). Immersing **xF-MAC-3** into different solvents (e.g. dichloromethane, methanol, acetone, ethyl acetate) for 2 h, PXRD patterns show no significant changes, indicating that **xF-MAC-3** has good solvent stability and the fluorine-functionalized of the ligands doesn't affect the solvent stability of the **MAC-3** structure (Fig. S5).

3.4 Gas adsorption properties

The N₂-77 K adsorption isotherms of **xF-MAC-3** reveal the presence of microporous structures in the structures. The BET surfaces are 532 m²g⁻¹ (**MAC-3**), 459 m²g⁻¹ (**2F-MAC-3**) and 579 m²g⁻¹ (**4F-MAC-3**, Fig. 3a), respectively. For the channel of **xF-MAC-3** is occupied by cationic CH₃NH₃⁺ molecules, the experimental BET surfaces are remarkably lower than the theoretical accessible surfaces calculated by Material Studio (van der Waals radius of the probe molecule: 1.84 Å; calculated supercell: 2 × 2 × 2 supercell)^[44]. The void space of **xF-MAC-3** is calculated by PLATON software and the data are listed in Table S2^[45]. The pore size distribution of **xF-MAC-3** is calculated by DFT model and the maximum pore sizes of **xF-MAC-3** are 5.52 Å (**MAC-3**), 5.88 Å (**2F-MAC-3**) and 5.73 Å (**4F-MAC-3**, Fig. 4b), respectively.

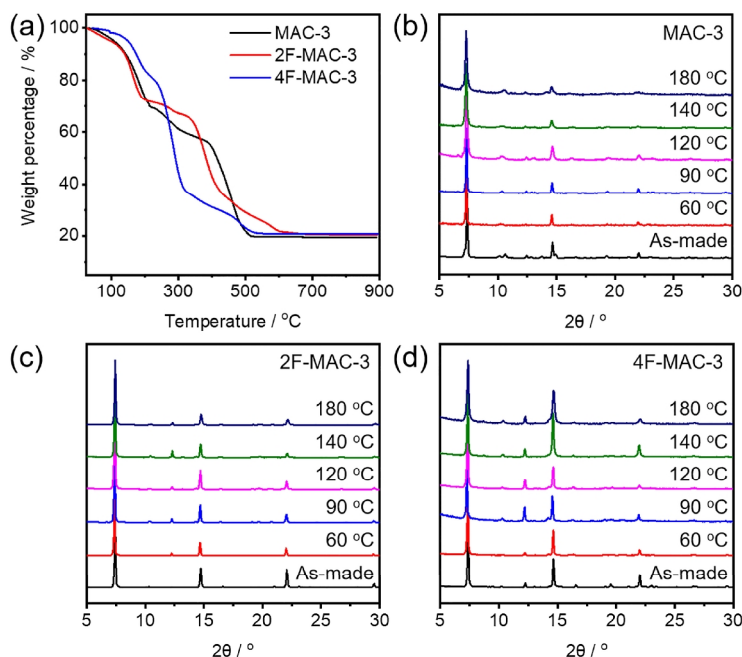


Fig. 3. (a) TGA curves; (b) Variable temperature PXRD patterns of **xF-MAC-3**

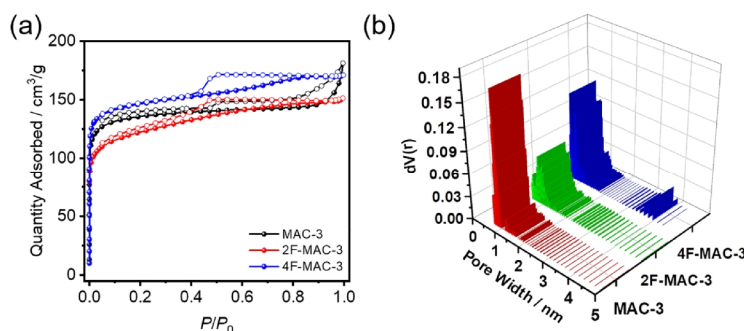


Fig. 4. (a) N₂-77K adsorption isotherms; (b) Pore size distribution of xF-MAC-3

H₂ and CO₂ adsorption experiments have been used to understand the relationship between gas adsorption capacity and fluorination degree of xF-MAC-3. CO₂-273 K adsorption experiments of xF-MAC-3 are carried out under 800 mmHg and the uptake of xF-MAC-3 amount is 23.21 cm³·g⁻¹ (1.04

mmol·g⁻¹, **MAC-3**), 27.50 cm³·g⁻¹ (1.23 mmol·g⁻¹, **2F-MAC-3**) and 36.13 cm³·g⁻¹ (1.61 mmol·g⁻¹, **4F-MAC-3**) respectively, which show that CO₂ uptake amount increases when fluorination degree increases on the carboxylate ligands (Fig. 5a~c).

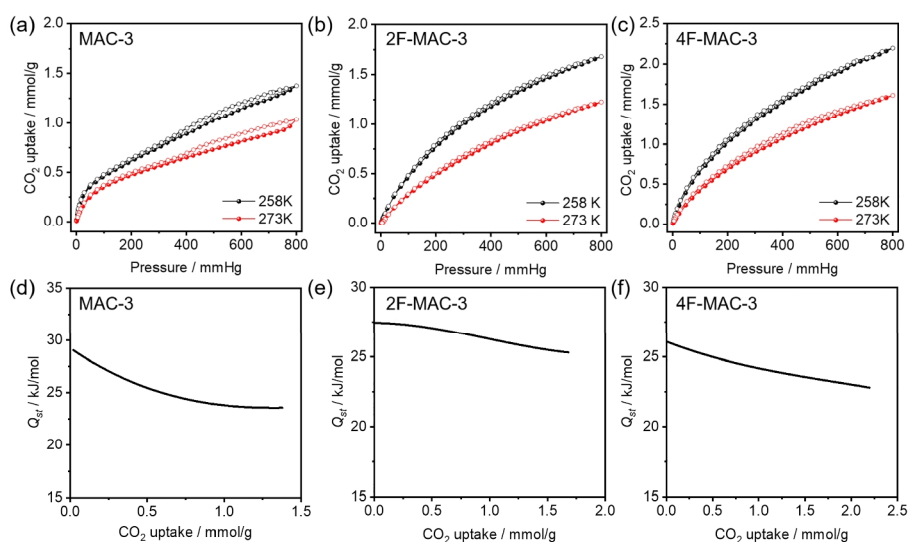


Fig. 5. (a) Low-pressure CO₂ adsorption isotherm at 258 and 273 K (solid line: adsorption isotherm; hollow line: desorption isotherm); (b) Adsorption heat (Q_{st}) for xF-MAC-3

To further investigate the effect of fluorination degree on CO₂ adsorption enthalpy (Q_{st}), we perform 258 K CO₂ adsorption experiments and the isosteric heat of CO₂ adsorption is calculated from the Virial method (Fig. S6, Fig. 5d~f)^[46]. The near-zero coverage Q_{st} is 29.0, 27.5 and 26.1 kJ·mol⁻¹ for **MAC-3**, **2F-MAC-3** and **4F-MAC-3**, respectively. The result illustrates that the interaction between the host xF-MAC-3 frameworks and guest CO₂ molecules adsorption decrease as the degree of fluorination increases, which is caused by the lower electronic density on the benzene ring after using fluorine-functionalized ligands^[42].

H₂-77 K adsorption experiment results show that the gas uptake amounts of xF-MAC-3 increase from 24.33 cm³·g⁻¹ (**MAC-3**) to 59.79 cm³·g⁻¹ (**4F-MAC-3**) at 77 K and 1 atm

(Fig. S7). Although the H₂ uptake amounts of xF-MAC-3 are significantly lower than some classical electrically neutral frameworks due to the presence of anti-balance cation in the channel of structures, **4F-MAC-3** has the highest H₂ capacity among the ionic fluorinated-MOFs^[31, 47]. It is further demonstrated that the structural pore properties and adsorption performance can be tuned by functionalization of ligands in MOF materials.

4 CONCLUSION

In conclusion, we synthesized three different fluorination degree MOFs (xF-MAC-3) with *pcu-b* topology. Our studies revealed that the introduction of fluorine atoms into

carboxylate ligands would not only enlarge the torsion angle φ of ligands but also elevate the space group of **xF-MAC-3**, which indicated that fluorination is crucial for MOFs structures. Besides, the CO₂ and H₂ adsorption abilities of **xF-MAC-3** have a great enhancement after fluorination, in which the H₂-77 K uptake of **4F-MAC-3** (59.79 cm³·g⁻¹) is

the highest among all anion fluorinated MOFs. Therefore, we do a systematic research on the effect of fluorination in **xF-MAC-3**, thus offering a potential way to study the ligand pre-functionalization effect on the structures and properties of MOFs analogues.

REFERENCES

- (1) Batten, S. R.; Champness, N. R.; Chen, X. M.; Garcia-Martinez, J.; Kitagawa, S.; Öhrström, L.; O'keeffe, M.; Suh, M. P.; Reedijk, J. Coordination polymers, metal-organic frameworks and the need for terminology guidelines. *CrystEngComm*. **2012**, 14, 3001–3004.
- (2) Batten, S. R.; Champness, N. R.; Chen, X. M.; Garcia-Martinez, J.; Kitagawa, S.; Öhrström, L.; O'keeffe, M.; Paik Suh, M.; Reedijk, J. Terminology of metal-organic frameworks and coordination polymers (Iupac Recommendations 2013). *Pure Appl. Chem.* **2013**, 85, 1715–1724.
- (3) Kalmutzki, M. J.; Hanikel, N.; Yaghi, O. M. Secondary building units as the turning point in the development of the reticular chemistry of MOFs. *Sci. Adv.* **2018**, 4, eaat9180.
- (4) Li, J. R.; Kuppler, R. J.; Zhou, H. C. Selective gas adsorption and separation in metal-organic frameworks. *Chem. Soc. Rev.* **2009**, 38, 1477–1504.
- (5) Zhao, X.; Wang, Y. X.; Li, D. S.; Bu, X. H.; Feng, P. Y. Metal-organic frameworks for separation. *Adv. Mater.* **2018**, 30, 1705189.
- (6) Lin, R. B.; Xiang, S. C.; Xing, H. B.; Zhou, W.; Chen, B. L. Exploration of porous Metal-organic frameworks for gas separation and purification. *Coord. Chem. Rev.* **2019**, 378, 87–103.
- (7) Lee, J.; Farha, O. K.; Roberts, J.; Scheidt, K. A.; Nguyen, S. T.; Hupp, J. T. Metal-organic framework materials as catalysts. *Chem. Soc. Rev.* **2009**, 38, 1450–1459.
- (8) Dhakshinamoorthy, A.; Li, Z. H.; Garcia, H. Catalysis and photocatalysis by metal organic frameworks. *Chem. Soc. Rev.* **2018**, 47, 8134–8172.
- (9) Jiao, L.; Wang, Y.; Jiang, H. L.; Xu, Q. Metal-organic frameworks as platforms for catalytic applications. *Adv. Mater.* **2018**, 30, 1703663.
- (10) Chen, B. L.; Xiang, S. C.; Qian, G. D. Metal-organic frameworks with functional pores for recognition of small molecules. *Acc. Chem. Res.* **2010**, 43, 1115–1124.
- (11) Lustig, W. P.; Mukherjee, S.; Rudd, N. D.; Desai, A. V.; Li, J.; Ghosh, S. K. Metal-organic frameworks: functional luminescent and photonic materials for sensing applications. *Chem. Soc. Rev.* **2017**, 46, 3242–3285.
- (12) Wu, S. Y.; Min, H.; Shi, W.; Cheng, P. Multicenter metal-organic framework-based ratiometric fluorescent sensors. *Adv. Mater.* **2020**, 32, 1805871.
- (13) Pachfule, P.; Banerjee, R. Fluorinated metal-organic frameworks (FMOFs): concept, construction, and properties. *Encyclopedia of Inorganic and Bioinorganic Chemistry*. New York; John Wiley & Sons, Ltd. **2014**.
- (14) Schloder, T.; Kraus, F.; Riedel, S. Fluorides: solid-state chemistry. *Encyclopedia of Inorganic and Bioinorganic Chemistry*. New York; John Wiley & Sons, Ltd. **2014**.
- (15) Noro, S.; Nakamura, T. Fluorine-functionalized metal-organic frameworks and porous coordination polymers. *NPG Asia Mater.* **2017**, 9, e433.
- (16) Cadiau, A.; Adil, K.; Bhatt, P. M.; Belmabkhout, Y.; Eddaoudi, M. A metal-organic framework-based splitter for separating propylene from propane. *Science* **2016**, 353, 137–140.
- (17) Cui, X. L.; Chen, K. J.; Xing, H. B.; Yang, Q. W.; Krishna, R.; Bao, Z. B.; Wu, H.; Zhou, W.; Dong, X. L.; Han, Y.; Li, B.; Ren, Q. L.; Zaworotko, M. J.; Chen, B. L. Pore chemistry and size control in hybrid porous materials for acetylene capture from ethylene. *Science* **2016**, 353, 141–144.
- (18) Cui, X. L.; Niu, Z.; Shan, C.; Yang, L. F.; Hu, J. B.; Wang, Q. J.; Lan, P. C.; Li, Y. J.; Wojtas, L.; Ma, S. Q.; Xing, H. B. Efficient separation of xylene isomers by a guest-responsive metal-organic framework with rotational anionic sites. *Nat. Commun.* **2020**, 11, 5456–5463.
- (19) Lin, Z. T.; Liu, Q. Y.; Yang, L.; He, C. T.; Li, L.; Wang, Y. L. Fluorinated biphenyldicarboxylate-based metal-organic framework exhibiting efficient propyne/propylene separation. *Inorg. Chem.* **2020**, 59, 4030–4036.
- (20) Fujie, K.; Otsubo, K.; Ikeda, R.; Yamada, T.; Kitagawa, H. Low temperature ionic conductor: ionic liquid incorporated within a metal-organic framework. *Chem. Sci.* **2015**, 6, 4306–4310.
- (21) Yang, C.; Wang, X. P.; Omary, M. A. Fluorous metal-organic frameworks for high-density gas adsorption. *J. Am. Chem. Soc.* **2007**, 129, 15454–12955.
- (22) Zhang, D. S.; Chang, Z.; Li, Y. F.; Jiang, Z. Y.; Xuan, Z. H.; Zhang, Y. H.; Li, J. R.; Chen, Q.; Hu, T. L.; Bu, X. H. Fluorous metal-organic frameworks with enhanced stability and high H₂/CO₂ storage capacities. *Sci. Rep.* **2013**, 3, 3312–3318.

- (23) Fan, W. D.; Liu, X. P.; Wang, X.; Li, Y.; Xing, C. Y.; Wang, Y. T.; Guo, W. Y.; Zhang, L. L.; Sun, D. F. A fluorine-functionalized microporous In-MOF with high physicochemical stability for light hydrocarbon storage and separation. *Inorg. Chem. Front.* **2018**, 5, 2445–2449.
- (24) Vimont, A.; Goupil, J. M.; Lavalley, J. C.; Daturi, M.; Surble, S.; Serre, C.; Millange, F.; Ferey, G.; Audebrand, N. Investigation of acid sites in a zeotypic giant pores chromium(III) carboxylate. *J. Am. Chem. Soc.* **2006**, 128, 3218–3227.
- (25) Peikert, K.; Hoffmann, F.; Froba, M. Fluorine magic: one new organofluorine linker leads to three new metal-organic frameworks. *Crystengcomm.* **2015**, 17, 353–360.
- (26) Fan, W. D.; Yuan, S.; Wang, W. J.; Feng, L.; Liu, X. P.; Zhang, X. R.; Wang, X.; Kang, Z. X.; Dai, F. N.; Yuan, D. Q.; Sun, D. F.; Zhou, H. C. Optimizing multivariate metal-organic frameworks for efficient C₂H₂/CO₂ separation. *J. Am. Chem. Soc.* **2020**, 142, 8728–8737.
- (27) Pachfule, P.; Chen, Y.; Jiang, J.; Banerjee, R. Fluorinated meta-organic frameworks: a dvantageous for higher H₂ and CO₂ adsorption or not? *Chem. Eur. J.* **2012**, 18, 688–694.
- (28) Jasuja, H.; Burch, N. C.; Huang, Y. G.; Cai, Y.; Walton, K. S. Kinetic water stability of an isostructural family of zinc-based pillared metal-organic frameworks. *Langmuir* **2013**, 29, 633–642.
- (29) Cheplakova, A. M.; Kovalenko, K. A.; Vinogradov, A. S.; Karpov, V. M.; Platonov, V. E.; Fedin, V. P. A comparative study of perfluorinated and non-fluorinated UiO-67 in gas adsorption. *J. Porous Mat.* **2020**, 27, 1773–1782.
- (30) Hulvey, Z.; Wragg, D. S.; Lin, Z. J.; Morris, R. E.; Cheetham, A. K. Ionothermal synthesis of inorganic-organic hybrid materials containing perfluorinated aliphatic dicarboxylate ligands. *Dalton Trans.* **2009**, 1131–1135.
- (31) Hulvey, Z.; Falcao, E. H. L.; Eckert, J.; Cheetham, A. K. Enhanced H₂ adsorption enthalpy in the low-surface area, partially fluorinated coordination polymer Zn₃(triazole)₆(tetrafluoroterephthalate)₂(H₂O)₂·4H₂O. *J. Mater. Chem.* **2009**, 19, 4307–4309.
- (32) Hulvey, Z.; Ayala, E.; Furman, J. D.; Forster, P. M.; Cheetham, A. K. Structural diversity in coordination polymers composed of divalent transition metals, 2,2'-bipyridine, and perfluorinated dicarboxylates. *Cryst. Growth Des.* **2009**, 9, 4759–4765.
- (33) Ling, Y.; Chen, Z. X.; Zhai, F. P.; Zhou, Y. M.; Weng, L. H.; Zhao, D. Y. A zinc(II) metal-organic framework based on triazole and dicarboxylate ligands for selective adsorption of hexane isomers. *Chem. Commun.* **2011**, 47, 7197–7199.
- (34) Jones, R. L.; Rees, C. W. Mechanism of heterocyclic ring expansions. IV. Reaction of an imidazole, pyrazole, and 1,2,4-triazole with dichlorocarbene. *J. Chem. Soc. C* **1969**, 2251–2255.
- (35) Person, D. V.; Fitch, J. W.; Cassidy, P. E.; Kono, K.; Reddy, V. S. Polymers from 2,5-difluoroterephthalic acid.1. Polyesters. *React. Funct. Polym.* **1996**, 30, 141–147.
- (36) Sheldrick, G. M. Crystal structure refinement with SHELXL. *Acta Crystallogr. C* **2015**, 71, 3–8.
- (37) Spek, A. L. Platon squeeze: a tool for the calculation of the disordered solvent contribution to the calculated structure factors. *Acta Crystallogr. C* **2015**, 71, 9–18.
- (38) Zhang, W.; Xu, J.; Sun, Z. Special functions and synthesis of aromatic fluorine-containing compounds. *Fine and Specialty Chemicals* **2005**, 13, 1–4.
- (39) Seidel, C.; Ahlers, R.; Ruschewitz, U. Coordination polymers with tetrafluoroterephthalate as bridging ligand. *Cryst. Growth Des.* **2014**, 14, 3576–3586.
- (40) Wu, J. *Recent Applications of Fourier Transform Infrared Spectrometry*. 1st ed.: scientific and Technical Documents Publishing House **1994**.
- (41) Blatov, V. A.; Shevchenko, A. P.; Proserpio, D. M. Applied topological analysis of crystal structures with the program package Topospro. *Cryst. Growth Des.* **2014**, 14, 3576–3586.
- (42) Hulvey, Z.; Furman, J. D.; Turner, S. A.; Tang, M.; Cheetham, A. K. Dimensionality trends in metal-organic frameworks containing perfluorinated or nonfluorinated benzenedicarboxylates. *Cryst. Growth Des.* **2010**, 10, 2041–2043.
- (43) Smets, D.; Ruschewitz, U. How does the fluorination of the linker affect the structural chemistry of trimesate-based metal-organic frameworks (MOFs)? *Z. Anorg. Allg. Chem.* **2020**, 646, 1157–1167.
- (44) Sale, M.; Avdeev, M. 3DBVSMAPPER: a program for automatically generating bond-valence sum landscapes. *J. Appl. Crystallogr.* **2012**, 45, 1054–1056.
- (45) Spek, A. L. Single-crystal structure validation with the program PLATON. *J. Appl. Crystallogr.* **2003**, 36, 7–13.
- (46) Metropolis, N.; Rosenbluth, A. W.; Rosenbluth, M. N.; Teller, A. H.; Teller, E. Equation of state calculations by fast computing machines. *J. Chem. Phys.* **1953**, 21, 1087–1092.
- (47) Forrest, K. A.; Pham, T.; Georgiev, P. A.; Pinzan, F.; Cioce, C. R.; Unruh, T.; Eckert, J.; Space, B. Investigating H₂ sorption in a fluorinated metal-organic framework with small pores through molecular simulation and inelastic neutron scattering. *Langmuir* **2015**, 31, 7328–7336.